Site symmetry analysis of the 738 nm defect in diamond

S. W. Brown[a),b)] and S. C. Rand
Division of Applied Physics, 1049 Randall Laboratory, The University of Michigan, Ann Arbor, Michigan 48109-1120

(Received 9 February 1995; accepted for publication 2 June 1995)

Based on a detailed analysis of polarized Raman and luminescence measurements of a "mosaic" diamond film, symmetry properties of a ubiquitous point defect observed in diamond films are determined. Specifically, the defect, which gives rise to emission at 738 nm, is determined unequivocally to be a ⟨110⟩-oriented defect with the transition dipole moment of the center oriented along the ⟨110⟩ symmetry axis. These results represent the first analysis of the symmetry properties of this point defect and aid in the development of structural model of the center. © *1995 American Institute of Physics.*

I. INTRODUCTION

Semiconductor materials with band gaps ranging from the visible to the ultraviolet, historically referred to as wide band-gap semiconductors, have been extensively studied for potential applications in high-temperature electronics as well as for UV-visible emissive devices. Recent advances in the chemical vapor deposition (CVD) growth of diamond films at reduced temperatures and pressures have expanded the potential of diamond for use in optical and high-temperature electronic applications. An understanding of the optical and electronic properties of defects in diamond films is critical for the accurate evaluation of potential applications of CVD diamond-based devices because of the significant effects of small point defect concentrations on the optical and electronic properties of these films. Many of the prominent defects observed in bulk diamond have been observed in as growth and ion-implanted diamond films. In this work, the symmetry properties of a ubiquitous infrared center in diamond films with a characteristic emission peak in the range from 1.67 to 1.684 eV (~738 nm) are discussed.

Strong narrow-line luminescence at 738 nm has been observed from diamond films grown by a variety of techniques including microwave-assisted CVD,[1–5] filament-assisted CVD,[6–9] plasma torch CVD,[9] and close-cycle thermal CVD.[10] The physical nature of this particular center is currently controversial. There are three known optically active point defects previously observed in bulk diamond with zero phonon lines which have energies in the range from 1.67 to 1.68 eV: a tetragonal defect with a zero phonon line at 1.684 eV (736 nm),[11] the neutral vacancy center (GR1) at 1.673 (741 nm),[11–14] and a silicon-related defect at 1.681 eV (737.5 nm).[2,10] Consequently, it is important to briefly review previous spectroscopic studies of point-defect centers in bulk diamond with emission features in this region, as well as properties of the unknown center found in diamond films.

Previous work[11] established that the tetragonal defect is not seen in cathodoluminescence, anneals out at temperatures above 700 K, and is not observed in luminescence at temperatures below 80 K. Cathodoluminescence (CL) attributable to the 738 nm defect in diamond films, on the other hand, has routinely been observed.[2,4,5,15] Also, temperature-dependent luminescence measurements show luminescence from the 738 nm center increasing in intensity as the temperature is decreased from 77 to 6 K. Finally, annealing experiments have shown that the 738 nm center is thermally stable up to annealing temperatures of 1700 K.[4] Based on these results, the 738 nm center is apparently not the tetragonal defect observed in bulk diamond.

Several groups[3,6,8] have postulated that the 738 nm emission originates from the strain-shifted neutral vacancy (GR1) located at 741 nm in bulk diamond. One claim against the 738 nm line being due to the GR1 center is that the annealing behavior of the 738 nm line is very different from that observed for the GR1 center. According to Davies,[13] the neutral vacancy anneals out at 900 K in type Ia diamond, and at 1200 K in type II diamond. In 1980, Vavilov *et al.*[10] published results of annealing studies of homoepitaxial diamond films which showed that the 738 nm emission was stable up to annealing temperatures of 1700 K. Similarly, Ruan *et al.*[4] reported that the 738 nm emission is stable up to an annealing temperature of 1650 K in microwave plasma-assisted CVD films. The annealing behavior of nitrogen-related defects in diamond films is, however, different from the annealing behavior of the defects in bulk diamond. For example, the 441 and 389 nm features both anneal out at temperatures below 1700 K in ion-implanted bulk diamond, yet are stable at 1700 K in diamond films.[10] Because of the anomaly, assignment of the 738 nm center to the GR1 center may not be ruled out based solely on the annealing behavior of the center.

Doping studies have also been done to elucidate the origin of the 738 nm emission. Yokota *et al.*[5] studied the effects of nitrogen on the CL spectrum of microwave plasma CVD diamond films grown on silicon substrates using 15% carbon monoxide in hydrogen as the source gas, with nitrogen introduced separately for doping. Luminescence at 738 nm was found to increase with moderate amounts of nitrogen and then decrease for higher concentrations of nitrogen. No luminescence was observed at 738 nm in the absence of nitrogen. While these results seemed to indicate that nitrogen may be involved in the center, Yokota nevertheless attributed the 738 nm line to a neutral vacancy center.

a)Electronic mail: brown@bloch.nrl.navy.mil
b)Present address: Naval Research Laboratory, Washington, DC 20375.

 0021-8979/95/78(6)/4069/7/$6.00

On the other hand, in their interpretation of results of a silicon ion implantation study, Vavilov *et al.*[10] attributed the origin of the 738 nm luminescence to a defect containing two interstitial silicon atoms. Ruan *et al.*[4] presented CL spectra from films grown under similar conditions on different substrates and found that luminescence from the 738 nm line was much stronger in films grown on silicon than on other substrates. In view of this, the 738 nm luminescence was attributed by Ruan to a silicon-related defect.

Finally, in a separate experiment, Collins *et al.*[2] implanted silicon into both natural and synthetic diamond samples. All samples showed evidence of the GR1 center at 741 nm because of damage caused by ion implantation, but in addition revealed a separate point defect at 738 nm, which was postulated to be silicon related. Observation of luminescence from both the GR1 and the 738 nm center in the same sample weakened the earlier argument that the 738 nm luminescence was caused by a strain-shifted GR1 center. Moreover, the strength of the line was strongest in a sample which contained significant amounts of isolated nitrogen atoms and was too weak to be observed in a sample with negligible nitrogen content. Based on these results, Collins attributed the 1.681 eV line to a center involving both silicon and nitrogen.

Three distinct models of the point defect responsible for the 738 nm luminescence feature therefore remain, the neutral vacancy, a center involving silicon alone (singly or as a di-silicon center), and a center involving silicon and nitrogen. In view of the divergent interpretations of available data, additional information about the physical and electronic structure of the center is clearly needed to develop a definitive structural model of this center.

Polarized luminescence has been used with great success in the past to establish site symmetries of prominent point defects. In diamond itself, for example, polarized luminescence measurements have previously been made on a number of defect centers, including the GR1 center a 1.673 eV, the N-V center at 1.94 eV, the H3 center at 2.46 eV, and the H4 center at 2.498 eV.[16–18] In the present work, polarized luminescence measurements were performed on a "mosaic" (quasi-single-crystal) diamond film which exhibited strong 738 nm luminescence in order to compare its emission with predictions based on various point group symmetries. Polarized Raman measurements of the mosaic diamond sample were used to establish the orientation of the film and to estimate the degree of orientational disorder of individual grains of the film. These results provide the first site symmetry analysis of this important point defect in CVD diamond films.

In Sec. II, a theoretical deviation of polarized Raman and luminescence results presented in this work is given. Experimental details are given in Sec. III. Finally, results are presented and discussed in Sec. IV.

II. THEORY

A. Polarized Raman

In the following discussion, an analysis of nonresonant polarized Raman scattering, where both incident and scattered photon energies are assumed to be far from any electronic resonance, is presented. Since Raman scattering is a second order process, the intensity of the Raman scattering is related to the second order polarizability tensor χ and the polarizations of the incident and scattered polarization vectors, $\mathbf{e_i}$ and $\mathbf{e_s}$, by the expression[19]

$$I_s \propto A I_i \sum_j \int (e_s \cdot \chi^j \cdot e_i)^2 d\Omega_s . \tag{1}$$

The constant prefactor A includes the dependence of the Raman scattering efficiency on the incident optical frequency ω_i and the cube of the scattered optical frequency ω_s. I_i refers to the intensity of the incident light, polarized in the $\mathbf{e_i}$ direction. The polarization dependence of the Raman intensity is then determined by the square of the contraction of the incident and scattered polarization vectors with the second-order polarizability tensor, summed over possible Raman modes (labelled with index j), and integrated over the detection solid angle.

The symmetry properties of χ are determined by the spatial symmetry of the sample being probed, formally specified by its symmetry group. In diamond, with two carbon atoms per unit cell and O_h symmetry, the three optic modes are Raman active and form a triply degenerate vibrational mode with F_{2g} symmetry at the center of the Brillouin zone. This mode has a room-temperature shift of 1332.5 ± 0.5 cm^{-1} and a measured linewidth of 1.76 ± 0.2 cm^{-1}.[20] Individual polarizability tensors for the triply degenerate F_{2g} mode are[21]

$$\chi^1 = \begin{bmatrix} 0 & 0 & 0 \\ 0 & 0 & d \\ 0 & d & 0 \end{bmatrix}, \quad \chi^2 = \begin{bmatrix} 0 & 0 & d \\ 0 & 0 & 0 \\ d & 0 & 0 \end{bmatrix}, \quad \chi^3 = \begin{bmatrix} 0 & d & 0 \\ d & 0 & 0 \\ 0 & 0 & 0 \end{bmatrix}. \tag{2}$$

In the following derivation, integration over the detection solid angle was ignored and the Raman intensity was calculated from Eq. (1) using the polarizability tensors given in Eq. (2). For a backscattering geometry, with incident and scattered propagation vectors along the z direction, $\mathbf{e_i}$ and $\mathbf{e_s}$ must lie in the xy plane, and only χ^3 gives a nonzero contribution to the Raman intensity. For the specific case where the polarizations of incident and scattered light remained fixed while the sample is rotated about the $\hat{z}$ axis, it is convenient to transform the crystallographic axes into the laboratory reference frame by the appropriate coordinate transformation: $\chi' = R\chi R^{-1}$, where R and R^{-1} are standard rotation matrices given by

$$R = \begin{bmatrix} \cos\theta & \sin\theta & 0 \\ -\sin\theta & \cos\theta & 0 \\ 0 & 0 & 1 \end{bmatrix},$$

and

$$R^{-1}=\begin{bmatrix}\cos\theta & -\sin\theta & 0\\ \sin\theta & \cos\theta & 0\\ 0 & 0 & 1\end{bmatrix}. \quad (3)$$

The polarizability tensor in the laboratory reference frame may then be expressed as

$$(\chi^3)'=d\begin{bmatrix}\sin 2(\theta+\theta_0) & -\cos 2(\theta+\theta_0) & 0\\ \cos 2(\theta+\theta_0) & -\sin 2(\theta+\theta_0) & 0\\ 0 & 0 & 0\end{bmatrix}, \quad (4)$$

where θ is the rotation of the crystal in the xy plane and θ_0 is the initial rotation between the laboratory and the crystallographic axes. The signal intensity I_s is therefore proportional to $\sin^2[2(\theta+\theta_0)]$ for co-polarized incident and scattered light and varies as $\cos^2[2(\theta+\theta_0)]$ for the cross-polarized case.

B. Polarized luminescence

The polarization dependence of the optical absorption and emission of point defects is determined by the point group of the center, which is a subgroup of the host crystal symmetry group. Subgroups of the point group T_d associated with points of the diamond lattice have previously been compiled by many authors.[19,21–24] These symmetry groups can be classified according to crystallographic groups and diamond point defects with five different symmetries can exist: tetragonal, trigonal, rhombic, monoclinic, and triclinic. Since the symmetry group of the center is a subgroup of the crystal, the symmetry axes of the center correspond to definite crystallographic directions. In particular, symmetry planes of the center coincide with those of the crystal, and symmetry axes of complex centers are directed along crystal axes of the same of higher order. Because of the existence of a definite orientation of the center with respect to the crystallographic axes, point defects may be conveniently grouped according to whether their highest symmetry axis lies along ⟨111⟩, ⟨110⟩, or ⟨100⟩ directions.[24]

The symmetry properties of the defect determine the nonzero transition matrix elements giving rise to optical selection rules which, in turn, lead to polarization effects both in absorption and in luminescence. To calculate the polarization properties of the luminescence from a point defect, therefore, it is necessary to multiply the absorption probability times the emission probability for each individual center and then sum over equivalent sites in the lattice.

To proceed with such calculations for centers of various possible structures, it is important to recognize that the orientation of their transition moments may either lie along the highest symmetry axis or perpendicular to it. These two possibilities are typically referred to as Z dipoles and XY dipoles corresponding to s-p_z and s-p_x,p_y electronic transitions, respectively, and must be considered separately in comparisons of the polarized luminescence intensities with calculations based on particular structural models. Once the orientation of the transition moment for the point group of a model of interest has been specified, its polarization pattern can be predicted following earlier work,[16–18,24,25] as outlined below.

It is convenient to use direction cosines in the evaluation of the polarization properties of point defects, oriented along $[\lambda\ \mu\ \nu]$. If the direction cosines of the incident electric field vector with respect to the symmetry axis of the point defect are $(l\ m\ n)$ and the direction cosines of the scattered radiation with respect to the same symmetry axis are $(l'\ m'\ n')$, the detected intensity of the luminescence may be written[16,25]

$$I=I_0\sum_i (l\lambda_i+m\mu_i+n\nu_i)^2(l'\lambda_i+m'\mu_i+n'\nu_i)^2. \quad (5)$$

I_0 is a constant which depends on the intensity of the incident light, as well as properties of the individual point defect such as the absorption cross section and luminescence efficiency. The first term in parentheses is proportional to the absorption probability while the second term is proportional to the emission probability. The sum is over equivalent sites in the crystal, labelled by the index i.

The luminescence intensity must be calculated for ⟨100⟩, ⟨110⟩, and ⟨111⟩-oriented point defects. There are three equivalent sites for ⟨100⟩-oriented point defects, ⟨100⟩, ⟨010⟩, and ⟨001⟩. For ⟨110⟩-oriented point defects there are six equivalent sites, namely, ⟨110⟩, ⟨101⟩, ⟨011⟩, ⟨1-10⟩, and ⟨01-1⟩. Finally, for ⟨111⟩-oriented point defects, there are four equivalent sites, namely ⟨111⟩, ⟨-1-11⟩, ⟨1-1-1⟩, and ⟨-11-1⟩.

In the following derivation, the polarization-dependent luminescence intensity is calculated for two specific situations, the case in which the incident polarization is rotated while the sample and the scattered polarization remain fixed and the case in which the incident and scattered polarizations remain fixed while the sample is rotated. When the incident polarization is rotated, the intensity dependence of the signal is calculated for a sample orientated such that the detected polarization is fixed along a ⟨100⟩ crystallographic direction, as well as along a ⟨110⟩ direction. Similarly, when the sample is rotated, the intensity dependence is calculated for both co-polarized and cross-polarized incident and scattered radiation.

Before proceeding with this calculation, we note that a simpler expression than that given by Eq. (5) was derived by Elliott *et al.*[25] For Z dipoles this simplified relation for the polarized emission intensity is given by the expression

$$I=I_0\left\{\sum_i l_i^2 l_i'^2+\left[\sum_i \lambda_i^2\mu_i^2\right]\left[1+2\left(\sum_i l_i l_i'\right)^2-5\sum_i l_i^2 l_i'^2\right]\right\}, \quad (6)$$

with a similar expression for XY dipoles

$$I=I_0\left\{1+\sum_i l_i'^2+\left[\sum_i \lambda_i^2\mu_i^2\right]\left[1+2\left(\sum_i l_i l_i'\right)^2-5\sum_i l_i^2 l_i'^2\right]\right\}. \quad (7)$$

In these equations, a shorthand notation was used for the summations over various orientations. The explicit meaning of the notation is

TABLE I. Dependence of the polarized luminescence intensity as a function of the angle β between the incident field and the crystallographic x axis. Functional dependences of both Z- and XY-oriented dipoles are expressed for point defects along ⟨111⟩, ⟨110⟩, and ⟨100⟩ crystallographic directions. Specific cases are considered in which the analyzer is oriented along a crystallographic ⟨100⟩ direction (column II) and along a crystallographic ⟨110⟩ direction (column III).

Defect orientation	Luminescence intensity (100) orientation	Luminescence intensity (110) orientation
⟨111⟩		
Z	constant	$1+2\sin\beta\cos\beta$
XY	constant	$2+\sin\beta\cos\beta$
⟨110⟩		
Z	$1+\cos^2\beta$	$3+4\sin\beta\cos\beta$
XY	$5+\cos^2\beta$	$11+4\sin\beta\cos\beta$
⟨100⟩		
Z	$\cos^2\beta$	constant
XY	$1+\cos^2\beta$	constant

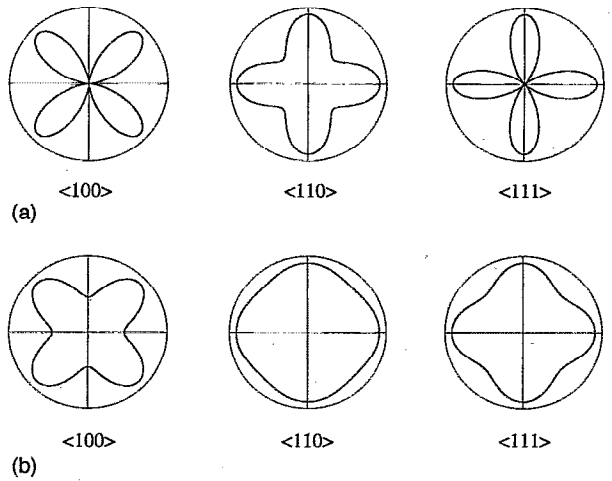

FIG. 1. Polar plots of theoretical calculations of the cross-polarized luminescence intensity as a function of sample rotation for (a) Z and (b) XY dipoles (see Table 2). The intensity dependences of point defects with symmetry axes oriented along ⟨111⟩, ⟨110⟩, and ⟨100⟩ directions are shown.

$$\sum_i l_i l_i' = (ll' + mm' + nn')$$

and

$$\sum_i \lambda_i^2 \mu_i^2 = (\lambda^2\mu^2 + \lambda^2\nu^2 + \nu^2\mu^2), \tag{8}$$

where, again, $(l\ m\ n)$ and $(l'\ m'\ n')$ are direction cosines of the incident and scattered light, and $[\lambda\ \mu\ \nu]$ refers to one of the equivalent point defect orientations in the crystal.

Expressions (6) and (7) are now applied to the specific cases discussed previously. Useful expressions for the polarized luminescence intensity were obtained for the experimental situation in which the incident polarization was rotated, while the sample as well as the orientation of the detected polarization remained fixed. These expressions for defects with symmetry axes aligned along ⟨111⟩, ⟨110⟩, and ⟨100⟩ crystallographic axes are compiled in Table I for the scattered polarization aligned parallel to both ⟨100⟩ and ⟨110⟩ crystallographic directions. Note the isotropic dependence of the luminescence intensity on the rotation of the incident polarization for a point defect with a symmetry axis along a ⟨111⟩ direction for the case where the detected polarization is aligned parallel to a crystallographic ⟨100⟩ direction. Similarly, a point defect with a symmetry axis along a ⟨100⟩ direction shows an isotropic dependence when the detected polarization is fixed along a crystallographic ⟨110⟩ direction.

Expressions resulting from an evaluation of Eq. (6) for the case in which the incident and scattered polarizations remain fixed while the sample is rotated are listed in Table 2. Polar plots of the dependence of the cross-polarized luminescence intensity on sample orientation listed in Table 2 appear in Fig. 1. Differences due to distinct assumed orientations of the transition moments (Z or XY dipoles) are evident in the figures.

III. EXPERIMENT

Measurements were made on a "mosaic" diamond film obtained from Kobe Steel USA Inc; details of the highly oriented nature of the diamond film have been previously described.[26] A scanning electron microscope (SEM) image of

TABLE II. Dependence of the polarized luminescence intensity as a function of sample rotation θ, for co- and cross-polarized light. Z- and XY-oriented dipoles are considered for point defects with symmetry axes along ⟨111⟩, ⟨110⟩, and ⟨100⟩ crystallographic directions. The detected polarization is aligned parallel to the ⟨100⟩ crystallographic direction for $\theta=0°$.

Defect orientation	Co-polarized intensity	Cross-polarized intensity
⟨111⟩		
Z	$1-\frac{2}{3}(\cos^4\theta+\sin^4\theta)$	$1-4\sin^2\theta\cos^2\theta$
XY	$2-\frac{2}{3}(\cos^4\theta+\sin^4\theta)$	$1-\sin^2\theta\cos^2\theta$
⟨110⟩		
Z	$3-(\cos^4\theta+\sin^4\theta)$	$1-2\sin^2\theta\cos^2\theta$
XY	$7-(\cos^4\theta+\sin^4\theta)$	$5-2\sin^2\theta\cos^2\theta$
⟨100⟩		
Z	$(\cos^4\theta+\sin^4\theta)$	$2\sin^2\theta\cos^2\theta$
XY	$1+(\cos^4\theta+\sin^4\theta)$	$1+2\sin^2\theta\cos^2\theta$

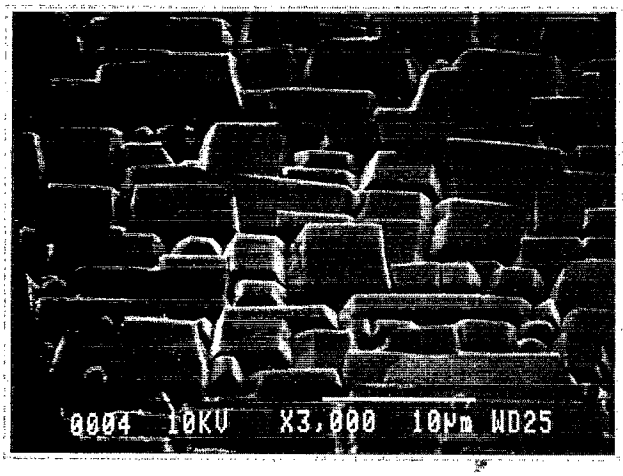

FIG. 2. SEM image of the "mosaic" diamond film.

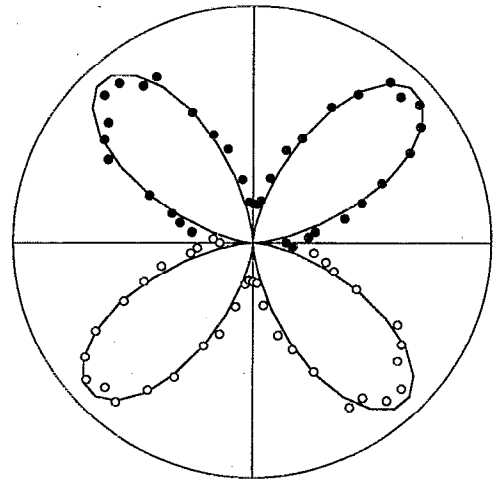

FIG. 3. Polar plot of the intensity dependence of the cross-polarized Raman signal from the "mosaic" diamond film as a function of the sample rotation θ. Solid circles represent the integrated intensity of the Raman signal whereas open circles are a guide to the eye, obtained by rotating the data through pi. The solid line is fit to the data using Eq. (4), with θ_0=47°.

the film surface, shown in Fig. 2, illustrates the oriented nature of the individual diamond crystallites comprising the polycrystalline film.

Polarized Raman measurements, made in a standard backscattering geometry, established the absolute orientation of the mosaic film and enabled an estimate of the degree of rotational misorientation of individual crystallites in the film to be made. In these experiments, 100 mW of 488 nm radiation from an argon ion laser was focused onto the sample with a 150 mm focal length lens. A small pick-off mirror in front of the collection lens steered the light onto the sample. Care was taken to ensure that the incident light was perpendicular to the plane of the sample and that only light scattered into a solid angle of 0.04 pi steradians about the backscattering direction reached the spectrometer. Polarizers fixed the incident and detected polarizations while samples were mounted on a calibrated rotation stage for rotation in the plane perpendicular to the wave vector of the incident light. A Spex TripleMate™ triple grating spectrometer dispersed the scattered radiation while an intensified diode array coupled with a signal digitizer allowed for rapid signal averaging; 500 scans were averaged for each data point.

Polarized luminescence measurements on the mosaic diamond film were performed with the experimental setup just described for polarized Raman measurements. In these experiments, 20 mW of 488 nm radiation from an argon ion laser was used to excite the sample and 30 scans were averaged for each data point. A series of polarized luminescence measurements were made where the incident polarization was rotated while the detected polarization remained fixed along sample ⟨100⟩ and ⟨110⟩ directions, respectively. In a second series of experiments, the incident and detected polarizations remained fixed, while the sample was rotated. All measurements were repeated a minimum of three times.

IV. RESULTS AND DISCUSSION

A polar plot of the cross-polarization Raman intensity as a function of sample rotation is shown in Fig. 3. In this figure, θ=0 corresponds to the incident electric field aligned along a silicon ⟨110⟩ direction. As theoretically described, for an experimental backscattering geometry where the polarizations of the incident and detected light are orthogonal to one another and the sample is rotated in the plane of polarization (the laboratory xy plane), the Raman intensity is proportional to $\cos^2[2(\theta+\theta_0)]$, where θ is the experimentally measured angle of rotation of the sample and θ_0 corresponds to the rotation of the sample ⟨100⟩ axis with respect to the laboratory x axis for θ=0°. A fit of the polarized Raman data shown in Fig. 3 to this expression gave an initial rotation θ_0 of 47° and established that the ⟨100⟩ plane of the mosaic diamond film was registered with the ⟨100⟩ plane of the silicon substrate, with the substrate cleaved along ⟨110⟩ axes. The fit to the data is shown as a solid line in the figure.

While there is almost a 10:1 ratio between the polarized Raman intensities for sample orientations of 0° and 45°, the nulls at 0° and 90° are incomplete, suggesting that the mosaic sample contains a small angular distribution of crystallites. A depolarized background contribution to the polarized Raman spectrum of 10% at the nulls is estimated to correspond to a random misorientation of the crystallites of approximately ±10° in the plane of the film. These results are in good agreement with previous polarized Raman measurements of similar highly oriented diamond films grown on silicon.[26,27] Based on the polarized Raman results, therefore, the mosaic diamond is highly ordered. Consequently, the results of polarized luminescence measurements can be compared directly with theoretical predictions to test proposed physical models of the center responsible for the 738 nm luminescence observed from diamond films.

The photoluminescence spectrum of the mosaic diamond sample is shown in Fig. 4. The spectrum was characterized by a broad emission band extending from 500 to 700 nm, as well as a sharp feature at 738 nm due to the defect center of interest. Polar plots of the dependence of the intensity of the 738 nm emission on the incident polarization are shown in Fig. 5. In Fig. 5(a), the dependence of the luminescence intensity on the incident polarization is shown for emission detected along a sample ⟨100⟩ direction. Similarly, Fig. 5(b)

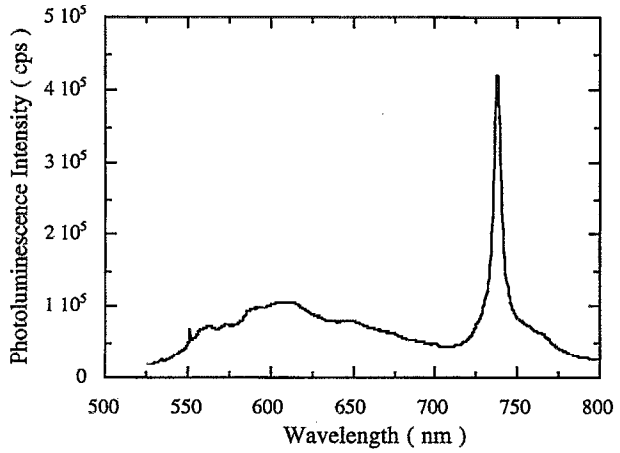

FIG. 4. Unpolarized photoluminescence spectrum of the "mosaic" diamond film.

shows the polarized luminescence intensity recorded as a function of the incident polarization for the detected polarization fixed along a sample ⟨110⟩ direction. As shown in Table I, ⟨100⟩-oriented defects are not expected to show any luminescence intensity dependence on the rotation of the incident polarization for the detector polarizer aligned parallel to a sample ⟨110⟩ direction. Similarly, luminescence from ⟨111⟩-oriented defects show an isotropic dependence on the incident polarization for the detector polarizer fixed along a

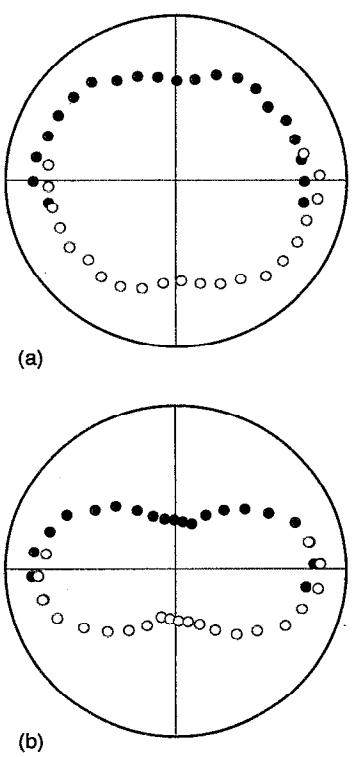

FIG. 5. Integrated intensity of the 738 nm emission as a function of the angle of rotation of the incident electric field. The analyzer remained fixed along (a) a sample ⟨100⟩ orientation and (b) a sample ⟨110⟩ orientation. Solid circles are experimental data while open circles represent the data rotated through pi. Thirty scans were averaged for each data point.

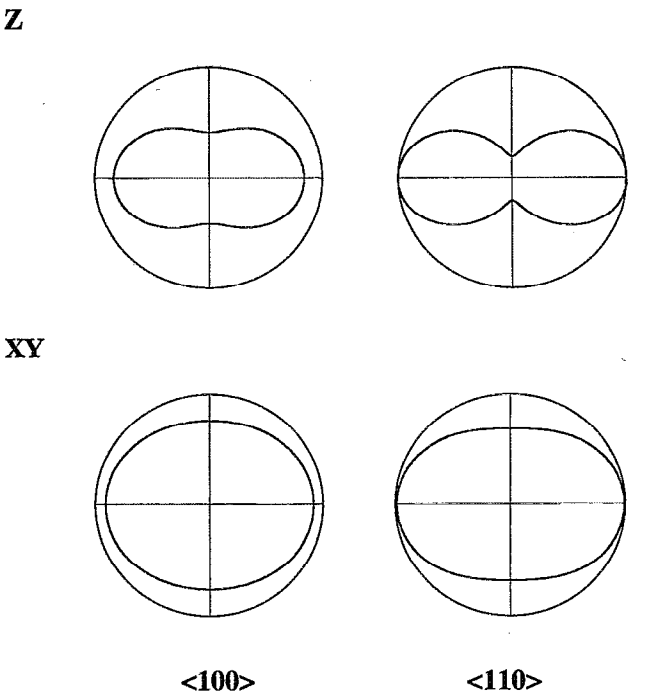

FIG. 6. Theoretical dependence of the polarized luminosity intensity as a function of sample rotation for (a) the analyzer aligned parallel to a ⟨100⟩ crystallographic orientation and (b) the analyzer aligned parallel to a ⟨110⟩ orientation. Dependences of both *Z* and *XY* dipoles are shown.

crystallographic ⟨100⟩ direction. Since the 738 nm emission showed a polarization dependence in both cases, the point defect giving rise to the 738 nm emission must have a ⟨110⟩ axis of symmetry.

A comparison of theoretical predictions for *Z* and *XY* dipoles with experimental results provides additional information about the symmetry of the center. Results of calculations based on the entries in Table I are plotted in Fig. 6 for both *Z* and *XY* dipoles. A direct comparison of Figs. 5 and 6 establishes that the dipole moment of the 738 nm center is aligned along the ⟨110⟩ symmetry axis (*Z* dipole).

Finally, a separate series of experiments was performed to confirm these results in which the incident and detected polarizations remained fixed while the sample was rotated in the plane of polarization. As shown in Fig. 7, a fourfold symmetric dependence on the sample rotation was observed, in good agreement with theoretically predicted results for a *Z* dipole oriented along a ⟨110⟩ symmetry axis, shown in Fig. 1.

Concerning the physical model of the center, previous polarized luminescence measurements established that the neutral vacancy GR1 center maintains the tetragonal T_d site symmetry of the lattice and tetragonal centers have symmetry axes oriented along ⟨100⟩ crystallographic directions.[18] These results therefore eliminate the GR1 center as a candidate for the origin of the 738 nm luminescence.

As discussed by Kaplyanskii,[24] point defects with type I rhombic and type I monoclinic symmetry both have rotational symmetry axes aligned along ⟨110⟩ directions: Rhombic I systems with ⟨110⟩ rotational symmetry axes have C_2

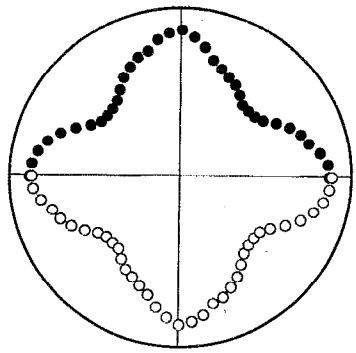

FIG. 7. Integrated luminescence intensity of the 738 nm emission as a function of the angle of rotation of the sample in the plane of polarization of the light for co-polarized light. A rotation of $\theta=0$ corresponds to the electric fields oriented along a sample ⟨110⟩ direction.

or σ_v ($\langle 110\rangle$) symmetry, with D_2 site symmetry and only Z oscillators are dipole allowed. Monoclinic I systems with ⟨110⟩ rotational symmetry axes have C_2 or $\sigma_h(\langle 110\rangle)$ symmetry. For these point defects, Z oscillators are allowed for C_2 point group symmetry and XY oscillators for σ_h point group symmetry.[11,24] Based on the experimental results, therefore, the defect giving rise to the 738 nm emission in diamond films belongs to the point group C_2 or D_2.

Two-atom point defects having ⟨110⟩ axes likely to be encountered in CVD diamond include a di-interstitial silicon pair, a di-interstitial silicon-nitrogen pair, and a substitutional silicon-vacancy pair, with the silicon atom occupying the next nearest-neighbor position. Point defects such as Si-V-Si or more complex centers oriented along a crystallographic ⟨110⟩ direction are also candidates for the impurity structure of the 738 nm center. However, polarized luminescence measurements are not by themselves adequate to distinguish between ⟨110⟩-oriented defect centers with D_2 and C_2 site symmetry. In this case, analysis of the 738 nm emission by an electric field or uniaxial stress is required.[11,24,28,29]

In summary, a detailed analysis of polarized luminescence measurements combined with polarized Raman measurements of a "mosaic" diamond film determined the dipole orientation and symmetry of a point defect ubiquitous to diamond films characterized by strong emission at 738 nm. Specifically, the defect was established to be a ⟨110⟩-oriented defect with either C_2 or D_2 symmetry, with the optical transition moment aligned along the ⟨110⟩ axis. These results represent the first site symmetry analysis of a point defect in a diamond film and eliminate the neutral vacancy (GR1) as the origin of the 738 nm emission.

ACKNOWLEDGMENTS

The authors would like to thank Bradley Fox and Kobe Steel USA Inc. for providing the mosaic diamond film used in this work. We would also like to thank Erdogan Gulari and Sadanand Deshpande of the University of Michigan for the generous loan of equipment necessary for the timely completion of this work. Partial support by the NSF Center for Ultrafast Optical Science (STC 8920108) is also acknowledged.

[1] A. T. Collins, Mater. Res. Soc. Symp. Proc. **162**, 3 (1990).
[2] A. T. Collins, M. Kamo, and Y. Sato, J. Mater. Res. **5**, 2507 (1990).
[3] B. G. Yacobi, A. R. Badzian, and T. Badzian, J. Appl. Phys. **69**, 1643 (1991).
[4] J. Ruan, W. J. Choyke, and W. D. Partlow, Appl. Phys. Lett. **58**, 295 (1991).
[5] Y. Yokota, H. Kawarada, and A. Hiraki, MRS Symp. Proc. **162**, 231 (1990).
[6] L. H. Robins, L. P. Cook, E. N. Farabaugh, and A. Feldman, Phys. Rev. B **39**, 13367 (1989).
[7] R. J. Graham, T. D. Moustakas, and M. M. Disko, J. Appl. Phys. **69**, 3213 (1991).
[8] J. E. Freitas, J. E. Butler, and U. Strom, J. Mater. Res. **5**, 2502 (1990); J. A. Freitas, U. Strom, J. E. Butler, and K. A. Snail, Proceedings of 2nd ICNDST, 1990.
[9] L. H. Robins, P. Tjossem, K. C. Smyth, P. Y. Barnes, E. N. Farabaugh, and A. Feldman, J. Appl. Phys. **69**, 3702 (1991).
[10] V. S. Vavilov, A. A. Gippius, A. M. Zaitsev, B. V. Deryagin, B. V. Spitsyn, and A. E. Alexsenko, Sov. Phys. Semicond. **14**, 1078 (1980).
[11] J. Walker, Rep. Prog. Phys. **42**, 108 (1979).
[12] G. Davies and C. M. Penchina, Proc. R. Soc. London Ser. A **338**, 359 (1974).
[13] G. Davies, Chem. Phys. Carbon **13**, 1 (1977).
[14] C. D. Clark and J. Walker, Proc. R. Soc. London Ser. A **334**, 241 (1973).
[15] B. G. Yacobi, A. R. Badzian, and T. Badzian, J. Appl. Phys. **69**, 1643 (1991).
[16] C. D. Clark, G. W. Maycraft, and E. W. J. Mitchell, J. Appl. Phys. **33**, 378 (1962), suppl.
[17] C. D. Clark and C. A. Norris, J. Phys. C **3**, 651 (1970).
[18] C. D. Clark and C. A. Norris, J. Phys. C **4**, 2221 (1971).
[19] R. Loudon, Adv. Phys. **13**, 423 (1964).
[20] S. A. Solin and K. Ramdas, Phys. Rev. B **1**, 1687 (1970).
[21] W. Hayes and R. Loudon, *Scattering of Light by Crystals* (Wiley, New York, 1978).
[22] M. Weissbluth, *Atoms and Molecules* (Academic, New York, 1978).
[23] M. Tinkham, *Group Theory and Quantum Mechanics* (McGraw–Hill, New York, 1964).
[24] A. A. Kaplyanskii, Opt. Spectrosc. **16**, 329 (1963); A. A. Kaplyanskii, Optika Spectrosk. **16**, 602 (1964).
[25] R. J. Elliott, I. G. Matthews, and E. W. Mitchell, Philos. Mag. **3**, 360 (1958).
[26] B. R. Stoner, D. M. Malta, A. J. Tessmer, J. Holmes, D. L. Driefus, R. C. Glass, A. Sowers, and R. J. Nemanich, *Diamond-Film Semiconductors* (SPIE, Bellingham, WA, 1994), Vol. 2151, p. 2.
[27] H.-J. Fuesser, M. Roesler, M. Hartweg, R. Zachai, X. Jiang, and C.-P. Klages, Proceedings of the Third International Symposium on Diamond Materials, 1993, Vol. 93, p. 102.
[28] G. Davies and M. H. Nazaré, J. Phys. C **13**, 4127 (1980).
[29] K. Mohammed, G. Davies, and A. T. Collins, J. Phys. C **15**, 2779 (1982).